Geotechnical Safety and Risk V
T. Schweckendiek et al. (Eds.)

doi:10.3233/978-1-61499-580-7-263

Slope Stability Assessment Based on Limit Analysis

Weigao WU
School of Engineering, University of Warwick, Coventry, United Kingdom

Abstract. Most of the research findings in evaluating slope stability using limit analysis are chart-based. No such stability chart is available to cover a wide range of material strength, slope geometries and external disturbance. Practitioners find it difficult to use the charts for a specific slope project. Compared with a large number of existing commercial softwares based on limit equilibrium and FEM, the practical use of limit analysis is not yet mature. In this paper, the development of a software package for slope stability assessment based on limit analysis is introduced. Several demonstrations of its features and verifications with a commercialized FEM software Phase2 are given. Slope stability assessment based on limit analysis is more efficient and can provide almost identical results compared with Phase2.

Keywords. Limit Analysis, Slope Stability, Software, Strength Reduction

1. Introduction

Generally speaking, there are three main methods for studying slope stability: limit equilibrium, displacement-based finite element method (FEM) and limit analysis. Limit equilibrium is the oldest technique for evaluating slope stability and has years of experience in practice. But the promotion of limit equilibrium is restricted by its arbitrary choice of failure mechanism and inter-slice forces. The FEM analysis, on the other hand, is a more rigorous and general approach. However, the FEM analysis is less attractive considering its dependence on mesh-density and computational capacity available. The concept of limit analysis was proposed by Drucker & Prager (1952) and was widely popularized in various geotechnical applications by Chen (1975). It should be noted that the application of limit analysis is still limited since most of the research findings are chart-based (e.g., Michalowski 1995, Utili 2013, Gao et al. 2014). Since no such stability chart is available to cover a wide range of material strength, slope geometries and external disturbance. Practitioners find it difficult to use the charts for a specific slope project. Compared with a large number of existing commercial softwares based on limit equilibrium and FEM, the practical use of limit analysis is not yet mature. In this paper, the development of a software package for slope stability assessment based on limit analysis is introduced. Several demonstrations of its features and verifications with a commercialized FEM software Phase2 (Rocscience 2005) are given.

2. Theoretical Basis

2.1. The Basics of Limit Analysis

In classic limit analysis, the material obeys a convex yield condition like Mohr-Coulomb failure criterion, and its plastic deformation is governed by the associative flow rule. The upper bound theorem of limit analysis is predominately used in solving the slope stability problems. Application of the kinematic approach requires equating the rate of work done by external disturbance (e.g., pore pressure, seismic forces and surface loads) and body forces to the internal energy dissipation rate for an assumed kinematically admissible failure mechanism. It can be expressed in the following equation

$$\int_{\Omega} \sigma'_{ij} \dot{\varepsilon}^*_{ij} d\Omega + \int_{\Gamma} \sigma'_{\Gamma'} \dot{\varepsilon}^*_{\Gamma} d\Gamma = WV^* + DV^* \qquad (1)$$

where the first term on the left-hand side of Eq. (1) is the rate of work done by the effective stress σ'_{ij} over the virtual strain rates $\dot{\varepsilon}^*_{ij}$, dissipated within Ω, the volume of the sliding soil/rock mass. The second left-hand side term is the internal energy dissipation along the slip surface Γ. The two terms on the right-hand side refer to the rates of work done by the weight of soil W and external disturbance D respectively. For simplicity, in this paper, the sliding soil/rock mass is assumed to be a rigid body, therefore, the first term on the left-hand side in Eq. (1) $\int_{\Omega} \sigma'_{ij}\dot{\varepsilon}^*_{ij} d\Omega = 0$. The principles to consider the energy dissipation within the sliding mass can be found in Chen (1975) and Donald & Chen (1997).

2.2. Strength Reduction Technique

To evaluate the margin of safety of a given slope, certain strength reduction techniques are provided to decrease the material strength until failure.

The shear strength reduction (SSR) technique is the most accepted method in slope stability assessment. For the material following Mohr-Coulomb failure criterion, both cohesion and frictional angle decrease simultaneously. The factor of safety is defined as

$$F_{SSR} = \frac{c}{c_m} = \frac{\tan\varphi}{\tan\varphi_m} \tag{2}$$

where c and ϕ are cohesion and internal frictional angle of the material respectively, c_m and ϕ_m are mobilized cohesion and internal friction angle for the slope to reach its critical stability. In the following formulation, the shear strength reduction technique is applied for the purpose of a general description. It should be noted other strength reduction techniques are also valid. For instance, Isakov et al. (2014) proposed that cohesion and frictional angle decrease at different rates, two-parameter factor of safety F_{double} is then defined as

$$F_{double} = \frac{1}{1 - R/\sqrt{2}} \tag{3}$$

where $R = \sqrt{\left(1-\frac{1}{F_c}\right)^2 + \left(1-\frac{1}{F_\phi}\right)^2}$, $F_c = \frac{c}{c_m}$, $F_\phi = \frac{\tan\varphi}{\tan\varphi_m}$.

2.3. Slope Stability Analysis Using Upper Bound Limit Analysis

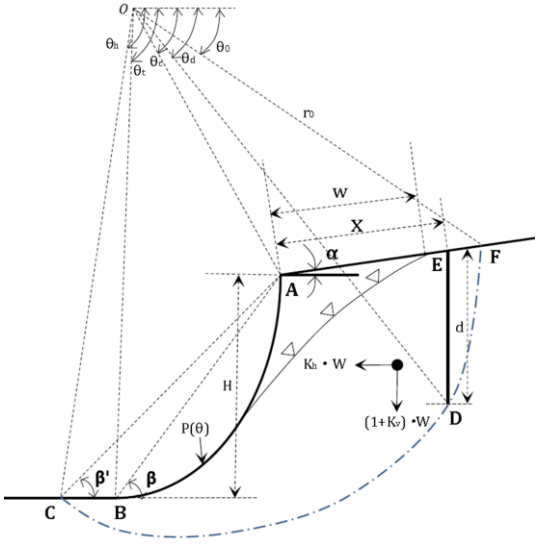

Figure 1. Failure mechanism.

According to Chen (1975), under the assumption that the material obeys Mohr-Coulomb failure criterion and normality flow rule, a logarithmic spiral failure surface is the most critical one among all kinematically admissible mechanisms. The equation of the failure surface in polar coordinates with reference to the spiral center ***O*** is

$$r = r_0 \cdot e^{\tan\phi_m \cdot (\theta - \theta_0)} \tag{4}$$

where r_0 is the radius of the log-spiral with respect to angle θ_0 (see Fig. 1). The sliding soil/rock mass (A-B-C-D-E) rotates as a rigid body about ***O*** with angular velocity $\dot{\omega}$, with the material below the log-spiral surface remaining at rest. The rate of work due to the material weight and pseudo-static seismic forces can be expressed as

$$\dot{W}_{inertia} = \gamma r_0^3 \dot{\omega} \begin{bmatrix} (1+K_v)(f_{1v} - f_{2v} - f_{3v} - f_{4v} - f_{5v} + f_{6v} - f_{7v}) \\ +K_h(f_{1h} - f_{2h} - f_{3h} - f_{4h} - f_{5h} + f_{6h} - f_{7h}) \end{bmatrix} \quad (5)$$
$$= \gamma r_0^3 \dot{\omega}\left[(1+K_v) f_v + K_h \cdot f_h\right]$$

with K_h and K_v, the horizontal and vertical seismic acceleration respectively, γ being the unit weight of the material. The detailed expressions for $f_{1v} \sim f_{7v}$ and $f_{1h} \sim f_{7h}$ are reported in the Appendix.

To account for water pressure within a slope, submerged or partially submerged, an extra team f_w is introduced.

An idealized hydraulic condition (Wylie & Mah 2004) is illustrated in Fig. 2. The flow lines are assumed to be straight lines with an inclination of $\arctan\left[H/(L+w\cdot\cos\alpha)\right]$ to horizontal axis. The assumed equipotentials are always vertical to the flow lines. Different position of x represents different submergence conditions from fully saturated to fully drained. f_w does not have a convenient closed form, and it is calculated numerically (see the Appendix).

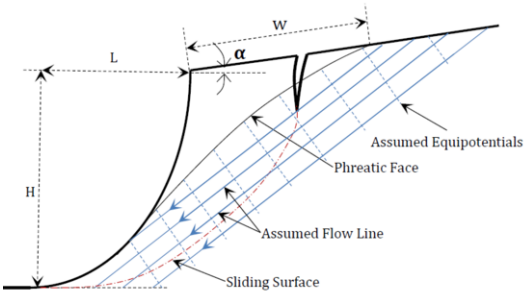

Figure 2. Idealized hydraulic condition.

Energy is dissipated only along the failure line C-D, and the rate of energy dissipation is obtained as

$$\dot{W}_d = c_m \omega r_0^2 e^{2\tan\phi_m(\theta_d-\theta_0)} \frac{e^{2\tan\phi_m(\theta_h-\theta_0)}-1}{2\tan\phi} \quad (6)$$
$$= c\omega r_0^2 f_d(\theta_0, \theta_d, \theta_h, \phi)$$

By equating the work rate of external forces to the internal energy dissipation rate, the stability factor can be defined as

$$N = \frac{\gamma H}{c_m} = \frac{f_d\left[e^{\tan\phi_m(\theta_h-\theta_0)}\cdot\sin\theta_h - \sin\theta_0\right]}{(1+K_v) f_v + K_h f_h + \frac{\gamma_w}{\gamma} f_w} \quad (7)$$

where γ_w is the unit weight of water.

The location of the log-spiral failure surface is determined by three parameters $\theta_0, \theta_h, \beta'$, which are regarded as variables. The most critical upper bound is found through an optimization procedure where the minimum value of the stability factor is sought. Since the factor of safety F appears on both sides of the Eq. (7), F can be found by an iterative procedure in which the resistance strength of the material are progressively changed according to Eq. (2), until

$$\frac{\gamma H}{c/F} = \frac{f_d\left[e^{\frac{\tan\phi}{F}(\theta_h-\theta_0)}\cdot\sin\theta_h - \sin\theta_0\right]}{(1+K_v) f_v + K_h f_h + \frac{\gamma_w}{\gamma} f_w}.$$

For materials following a non-linear failure criterion, Eq. (7) could be modified by using the equivalent cohesion and frictional angle (Wylie & Mah 2004) or the tangential technique proposed by Collins et al. (1988).

3. Sensitivity Analysis

The stability of a slope is governed by a range of factors such as material strength, slope geometry and external disturbance. All these factors are treated as known and deterministic variables in the stability evaluation. In fact, most of the factors are stochastic. Each factor has a different degree of impact on the slope stability. Thus, it is important to implement sensitivity analysis since it helps to establish the relationship between the safety of slope with each factor quantitatively. It is even more interesting to study the interaction between the factors and to determine the major/minor factors for slope instability.

The sensitivity analyses are mainly executed with limit equilibrium or FEM. Compared with limit analysis, long computational time and low efficiency when using the other two methods make them less attractive to carry out a comprehensive study for both one at a time or

multi-variable sensitivity analysis. In this paper, the present software is capable of running sensitivity analysis to assess the distinct influence of each factor in slope stability.

4. Development of a Software Package for Slope Stability Assessment

4.1. Framework

The framework of the software is quite straightforward (see Fig. 3). First of all, users should input the slope geometry, material properties and external forces. The slope geometry includes the inclination of the slope, height of slope, the radius of slope face, the position and depth of the crack and the position of water table. The material properties for a Mohr-Coulomb material include the unit weight, cohesion and frictional angle. Moreover, when Hoek-Brown failure criterion is chosen, the values of m_i , geological strength index (GSI) and disturbance coefficient (D) should be given. The external forces include the horizontal and vertical seismic forces. Three different strength reduction techniques are available to choose from. The interface of the input control panel is shown in Fig. 4.

After the input, the software calculates the factor of safety for the given slope automatically. In addition, the software can implement one-at-a time and multi-variables sensitivity analysis.

Finally, the software shows the failure mechanism for the given slope (see Fig. 5) and plots the variation of the factor of safety against different parameters.

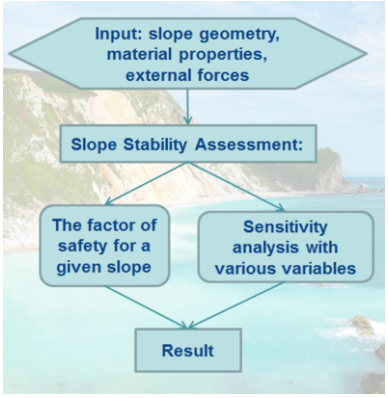

Figure 3. Framework of the software.

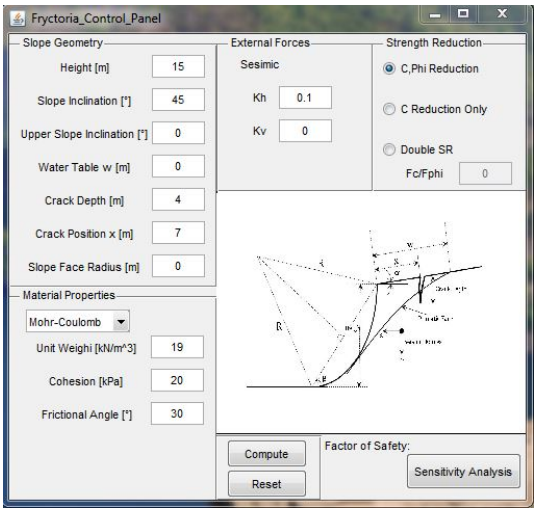

Figure 4. Interface: control panel.

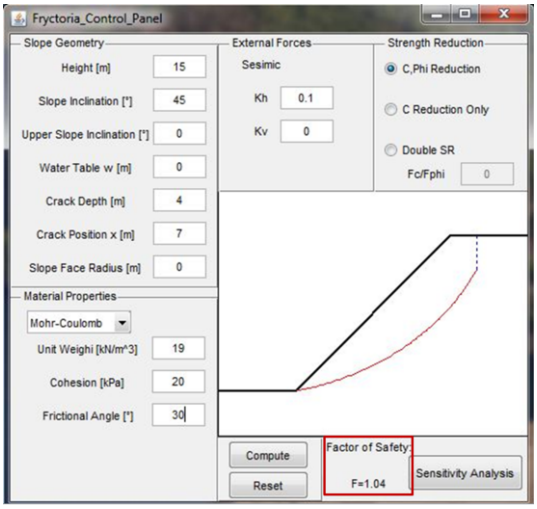

Figure 5. Result display: failure mechanism and the factor of safety.

4.2. Verification

The accuracy of the software is examined and verified by a commercialized finite-element software Phase2.

In Table 1~Table 3, the factor of safety against various values of frictional angles, cohesions and slope inclinations are presented. It is noted that the present software gives almost identical results compared with Phase2.

In Table 4 and Table 5, the impact of seismic forces and different positions of water table are inspected respectively. The present

software provides almost same results with different values of seismic accelerations. The difference in terms of pore pressure is more visible than any other factors. However, the present software always gives safer or more conservative results.

Table 1. Factor of safety against different values of frictional angle.

$\beta = 45°, H = 20m, c = 20kPa, \gamma = 19kN/m^3$								
$\emptyset$ (°)	10		15		20		25	
	Present Work	Phase2	Present Work	Phase2	Present Work	Phase2	Present Work	Phase2
FS	0.64	0.64	0.79	0.80	0.93	0.93	1.08	1.08
$\emptyset$ (°)	30		35		40			
	Present Work	Phase2	Present Work	Phase2	Present Work	Phase2		
FS	1.23	1.24	1.40	1.40	1.57	1.58		

Table 2. Factor of safety against different values of cohesion.

$\beta = 45°, H = 20m, \emptyset = 20°, \gamma = 19kN/m^3$								
$c\ (kPa)$	10		15		20		25	
	Present Work	Phase2	Present Work	Phase2	Present Work	Phase2	Present Work	Phase2
FS	0.71	0.72	0.83	0.83	0.93	0.93	1.03	1.03
$c\ (kPa)$	30		35		40			
	Present Work	Phase2	Present Work	Phase2	Present Work	Phase2		
FS	1.12	1.13	1.22	1.22	1.31	1.32		

Table 3. Factor of safety against different values of slope inclination.

$H = 20m, c = 20kPa, \emptyset = 20°, \gamma = 19kN/m^3$						
β (°)	30		40		50	
	Present Work	Phase2	Present Work	Phase2	Present Work	Phase2
FS	1.27	1.27	1.02	1.03	0.85	0.85
β (°)	60		70		80	
	Present Work	Phase2	Present Work	Phase2	Present Work	Phase2
FS	0.73	0.73	0.62	0.63	0.52	0.52

Table 4. Factor of safety against different values of seismic acceleration.

$\beta = 45°, H = 20m, c = 20kPa, \emptyset = 20°, \gamma = 19kN/m^3$						
k_h	0.1		0.15		0.2	
	Present Work	Phase2	Present Work	Phase2	Present Work	Phase2
FS	1.06	1.06	0.99	0.99	0.92	0.92
k_h	0.25		0.3			
	Present Work	Phase2	Present Work	Phase2		
FS	0.86	0.87	0.80	0.80		

Table 5. Factor of safety against different position of water table.

$\beta = 45°, H = 20m, c = 20kPa, \emptyset = 20°, \gamma = 19kN/m^3$						
w	0		H/4		H/2	
	Present Work	Phase2	Present Work	Phase2	Present Work	Phase2
FS	0.72	0.69	0.77	0.73	0.92	0.88
w	H		2H		4H	
	Present Work	Phase2	Present Work	Phase2	Present Work	Phase2
FS	1.09	1.04	1.21	1.20	1.22	1.21

5. Conclusion

The present software has the following advantages over softwares based on FEM.

First of all, the software widely extends the application of limit analysis. One of the reasons why limit analysis is less popular compared with limit equilibrium and finite element is the chart-based design approach. The stability charts only provide factor of safety or stability factor for a limited number of cases, making engineers reluctant to use for a specific and practical project.

Secondly, the results obtained from the FEM analyses largely depend on mesh density. However, the present software based on analytical limit analysis is mesh-independent.

More importantly, the present software has a higher computational efficiency than the FEM softwares. It takes much less time to reach a same level of precision. Due to its high efficiency, the present software makes automatic sensitivity analysis possible.

Finally, the theory of limit analysis and its applications are still improving and it is not difficult to include other features such as pile/anchor reinforcement and successive failure in future upgrades.

References

Chen, Wai-Fah (1975) Limit analysis and soil plasticity, Amsterdam ; Oxford: Elsevier.

Collins, I. F., C. I. M. Gunn, M. J. Pender, and W. Yan (1988) "SLOPE STABILITY ANALYSES FOR MATERIALS WITH A NON-LINEAR FAILURE ENVELOPE," International Journal for Numerical and Analytical Methods in Geomechanics, Vol. 12, No. 5, pp 533-550.

Donald, I. B., and Z. Y. Chen (1997) "Slope stability analysis by the upper bound approach: fundamentals and methods," Canadian Geotechnical Journal, Vol. 34, No. 6, pp 853-862.

Drucker, D.C., and Prager, W. (1952) “Soil mechanics and plastic analysis or limit design.” Quarterly of Appied Mathematics, Vol. 10, No. 2, pp 157-165.

Gao, Y. F., D. S. Zhu, F. Zhang, G. H. Lei, and H. Y. Qin (2014) "Stability analysis of three-dimensional slopes under water drawdown conditions," Canadian Geotechnical Journal, Vol. 51, No. 11, pp 1355-1364.

Isakov, A., and Y. Moryachkov (2014) "Estimation of Slope Stability Using Two-Parameter Criterion of Stability," International Journal of Geomechanics, Vol. 14, No. 3, p 3.

Michalowski, R. L. (1995) "Slope stability analysis: A kinematical approach," Geotechnique, Vol. 45, No. 2, pp 283-293.

Rocscience Inc. (2005) “Phase2 v6.0 – Two-Dimensional Finite Element Slope Stability Analysis,” Verification Manual.

Utili, S. (2013) "Investigation by limit analysis on the stability of slopes with cracks," Geotechnique, Vol. 63, No. 2, pp 140-154.

Wyllie, Duncan C., Christopher W. Mah, and Evert Rock slope engineering Hoek (2004) Rock slope engineering : civil and mining, London: Spon.

Appendix

$$\frac{H}{r_0}=\frac{\sin\beta'}{\sin(\beta'-\alpha)}\left[\sin(\theta_h+\alpha)e^{\tan\phi_m(\theta_h-\theta_0)}-\sin(\theta_0+\alpha)\right]$$

$$\frac{L_1}{r_0}=\frac{\sin(\theta_h-\theta_0)}{\sin(\theta_h+\alpha)}-\frac{\sin(\theta_h+\beta')}{\sin(\theta_h+\alpha)\sin(\beta'-\alpha)}\left[\sin(\theta_h+\alpha)e^{\tan\phi_m(\theta_h-\theta_0)}-\sin(\theta_0+\alpha)\right]$$

$$\frac{L_2}{r_0}=\frac{\sin(\theta_d-\theta_0)}{\sin(\theta_d+\alpha)}-\frac{\cos\theta_d\left[e^{\tan\phi_m(\theta_d-\theta_0)}\sin(\theta_d+\alpha)-\sin(\theta_0+\alpha)\right]}{\sin(\theta_d+\alpha)\cos\alpha}$$

$$\frac{\delta}{r_0}=\frac{e^{\tan\phi_m(\theta_d-\theta_0)}\sin(\theta_d+\alpha)-\sin(\theta_0+\alpha)}{\cos\alpha}$$

$$\theta_c=\operatorname{actan}\left(\frac{\sin\theta_0+L_1\sin\alpha/r_0}{\cos\theta_0-L_1\cos\alpha/r_0}\right)$$

$$\theta_t=\operatorname{actan}\left(\frac{\sin\theta_0+L_1\sin\alpha/r_0+H/r_0}{\cos\theta_0-L_1\cos\alpha/r_0-H/r_0/\tan\beta}\right)$$

$$f_{1v}=\frac{(3\tan\phi_m\cdot\cos\theta_h+\sin\theta_h)e^{3\tan\phi_m(\theta_h-\theta_0)}-3\tan\phi_m\cdot\cos\theta_0-\sin\theta_0}{3(1+9\tan^2\phi_m)}$$

$$f_{2v}=\frac{L_1}{6r_0}\left(2\cos\theta_0-\frac{L_1}{r_0}\cos\alpha\right)\cdot\sin(\theta_0+\alpha)$$

$$f_{3v}=\frac{1}{3}\int_{\theta_c}^{\theta_t}p^3(\theta)\cos\theta d\theta$$

$$f_{4v}=\frac{e^{3\tan\phi_m(\theta_d-\theta_0)}(3\tan\phi_m\cos\theta_d+\sin\theta_d)-3\tan\phi_m\cos\theta_0-\sin\theta_0}{3(1+9\tan^2\phi_m)}$$

$$f_{5v}=\frac{L_2\sin(\theta_0+\alpha)\cdot(2\cos(\theta_0+\alpha)-L_2/r_0)}{6r_0}$$

$$f_{6v}=\frac{\delta}{3r_0}e^{2\tan\phi_m(\theta_d-\theta_0)}\cos^2\theta_d$$

$$f_{7v}=\frac{H(\cot\beta'-\cot\beta)}{6r_0}\left(\frac{H}{r_0}+\sin\theta_0+\frac{L_1}{r_0}\sin\alpha\right)\left[2e^{\tan\phi_m(\theta_h-\theta_0)}\cos\theta_h-\frac{H}{r_0}(\cot\beta'-\cot\beta)\right]$$

$$f_{1h}=\frac{(3\tan\phi_m\cdot\sin\theta_h-\cos\theta_h)e^{3\tan\phi_m(\theta_h-\theta_0)}-3\tan\phi_m\cdot\sin\theta_0+\cos\theta_0}{3(1+9\tan^2\phi_m)}$$

$$f_{2h}=\frac{L_1}{6r_0}\left(2\sin\theta_0+\frac{L_1}{r_0}\sin\alpha\right)\cdot\sin(\theta_0+\alpha)$$

$$f_{3h}=\frac{1}{3}\int_{\theta_c}^{\theta_t}p^3(\theta)\sin\theta d\theta$$

$$f_{4h}=\frac{e^{3\tan\phi_m(\theta_d-\theta_0)}(3\tan\phi_m\cos\theta_d-\cos\theta_d)-3\tan\phi_m\sin\theta_0+\cos\theta_0}{3(1+9\tan^2\phi_m)}$$

$$f_{5h}=\frac{L_2\sin^2(\theta_0+\alpha)}{3r_0}$$

$$f_{6h}=\frac{\delta}{6r_0}e^{\tan\phi_m(\theta_d-\theta_0)}\cos\theta_d\left(2e^{\tan\phi_m(\theta_d-\theta_0)}\sin\theta_d-\frac{\delta}{r_0}\right)$$

$$f_{7h}=\frac{H(\cot\beta'-\cot\beta)}{3r_0}\left(\frac{H}{r_0}+\sin\theta_0+\frac{L_1}{r_0}\sin\alpha\right)e^{\tan\phi_m(\theta_h-\theta_0)}\sin\theta_h$$

$$f_w=\tan\phi_m\left[\int_{\theta_d}^{\theta_t}h_1e^{2\tan\phi_m(\theta-\theta_0)}d\theta+\int_{\theta_t}^{\theta_h}h_2e^{2\tan\phi_m(\theta-\theta_0)}d\theta+\int_{\theta_h}^{\theta_0}h_3e^{2\tan\phi_m(\theta-\theta_0)}d\theta\right]$$

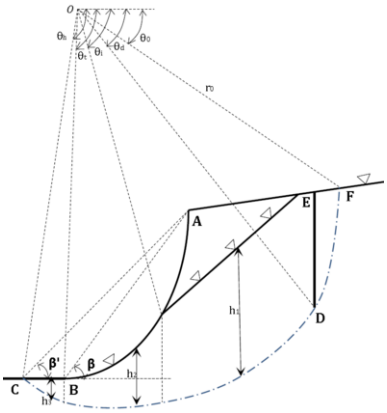

Figure 6. Slope under water pressure.